Research Article/Araştırma Makalesi

Gazi AKADEMİK YAYINCILIK

GAZİ
JOURNAL OF ENGINEERING SCIENCES

A Parametric Investigation on Various Compliant Inertial Amplification Mechanisms for a Periodic Vibration Isolator Design

Enes Er [a], **Erol Türkeş** [b], **Osman Yüksel** *[c]

Submitted: 28.07.2022 Revised: 25.10.2022 Accepted: 03.12.2022 doi:10.30855/gmbd.0705039

ABSTRACT

In this study, a vibration isolator is designed as a periodic structure, which is constructed with embedded inertial amplification mechanisms. At first, various compliant inertial amplification mechanism configurations are proposed. Among them, the one with the widest vibration isolation frequency band is selected via conducted parametric studies. Then, the determined mechanism is utilized as the unit cell (i.e., the repetitive building block) of the periodic structure. Finally, the displacement transmissibility (i.e., Frequency Response Function (FRF)) plots are presented to demonstrate the vibration isolation performance of the designed periodic structure. According to the numerical results, the selected unit cell mechanism provides more than 25 % vibration isolation between 190-360 Hz frequency values. On the other hand, the periodic structure formed with linearly incorporating three unit cell mechanisms provides more than 80 % vibration isolation for the same frequency range (i.e., 190-360 Hz). As a conclusion, if the number of unit cells used in the periodic structure is increased further, higher vibration isolation levels will be achieved for 190-360 Hz frequency range.

Keywords: Parametric study, compliant mechanism, vibration isolation, inertial amplification, periodic structure

[a] Kırklareli University, Faculty of Engineering, Dept. of Mechanical Engineering 39010 - Kırklareli, Türkiye
Orcid: 0000-0003-0429-4467
e mail: eneser9398@gmail.com

[b] Kırklareli University, Faculty of Engineering, Dept. of Mechanical Engineering 39010 - Kırklareli, Türkiye
Orcid: 0000-0002-9601-7119
e mail: erol.turkes@klu.edu.tr

[c,*] Kırklareli University, Faculty of Engineering, Dept. Of Mechanical Engineering, 39010 – Kırklareli, Türkiye
Orcid: 0000-0001-9492-1756
e mail: osmanyuksel@klu.edu.tr

*Corresponding author: osmanyuksel@klu.edu.tr

Çeşitli Esnek Atalet Artırımı Mekanizmalarının Periyodik Titreşim Yalıtıcısı Tasarımına Yönelik Parametrik İncelemesi

ÖZ

Bu çalışmada, iç içe gömülmüş atalet artırımı mekanizmalarıyla oluşturulmuş bir periyodik yapı, titreşim yalıtıcısı olarak tasarlanmıştır. İlk olarak, çeşitli esnek atalet artırımı mekanizma konfigürasyonları önerilmiştir. Yapılan parametrik çalışmalar neticesinde, bu mekanizmalardan en geniş titreşim yalıtımı frekans aralığına sahip olanı belirlenmiştir. Ardından, bu seçilen tasarım, periyodik yapının birim hücresi (periyodik yapıda tekrar eden yapı bloğu) olarak kullanılmıştır. Son olarak, periyodik yapının titreşim yalıtımı performansını göstermek için deplasman iletkenliği (frekans cevap fonksiyonu) grafikleri sunulmuştur. Sayısal çalışmaların sonuçlarına göre, seçilen birim hücre mekanizması 190-360 Hz frekans aralığında % 25'ten fazla titreşim yalıtımı sağlamaktadır. Öte yandan, üç adet birim hücre mekanizmasının doğrusal bir biçimde birleştirilmesiyle oluşturulan periyodik yapı, aynı frekans aralığında (190-360 Hz) % 80'den fazla titreşim yalıtımı sağlamaktadır. Sonuç olarak, periyodik yapıda kullanılan birim hücre sayısı daha da artırılırsa, 190-360 Hz frekans aralığında daha yüksek titreşim yalıtım düzeylerine ulaşılacaktır.

Anahtar Kelimeler: Parametrik çalışma, esnek bağlantılı mekanizma, titreşim yalıtımı, atalet artırımı, periyodik yapı

To cite this article: E. Er, E. Turkes and O. Yuksel, "A Parametric Investigation on Various Compliant Inertial Amplification Mechanisms for a Periodic Vibration Isolator Design," *Gazi Journal of Engineering Sciences*, vol. 8, no. 3, pp. 511-523, 2022. doi:10.30855/gmbd.0705039

1. Introduction

Mechanical vibrations are defined as the movement of waves around a certain equilibrium point. The movement in here occurs in a certain amplitude and period. These movements can both occur as harmonic or randomly distributed movement. If there is no damping or isolation for these waves in the system, then the vibration levels affecting the system can exceed the vibration level of the source. For this reason, an isolator for a mechanical structure is needed to reduce the vibration level of a system. Mechanical isolators prevent incoming source vibrations to reach the system, hence protect it from destructive oscillations. [1-3]

The most known traditional vibration isolation system is a mass-spring system. In these isolators, mechanical vibrations can be shown with the energy transformations of a system. Potential energy transforms to kinetic energy and after that it transforms to potential energy again. Therefore, a vibrating system must have components which store potential and kinetic energy. Springs and other similar elastic components are used for storage of potential energy. Similarly, mass and other inertia components used in these systems are able to store kinetic energy. [4-6]

Beside traditional vibration isolation methods, in recent years, innovative periodic structures [7, 8] were created to prevent the propagation of elastic and acoustic waves from the source to the target. Inertial amplification [9, 10] induced elastic metamaterials are a type of the innovative periodic structures [11, 12] which can inhibit vibration propagation. Therefore, this type of periodic structures can be utilized as vibration isolators [13-17]. Moreover, with these periodic structures, effective vibration isolation can be achieved for low frequency regions by altering their design parameters such as their size [18-20], shape [19], topology [20, 21].

In the literature, there exist various studies that examine vibration isolation properties of periodic structures constructed with different lumped and compliant inertial amplification mechanisms. In Ref. [22], enhanced tuned mass damper type vibration isolation system was designed by using a lumped parameter inertial amplification mechanism. In Ref. [23], vibration isolation enhancement in periodic nonuniform beams was achieved by introducing lumped parameter inertial amplification mechanisms. In Ref. [24], a amplification vibration isolator with periodic composite sandwich beams with lumped parameter inertial mechanisms was designed. In Ref. [25], vibration transmission reduction was attained in an elastic rod for a certain frequency range by periodically attaching lumped parameter inertial amplification mechanisms. The studies mentioned so far are all lumped parameter models. On the other hand, in the literature, there are numerous studies that investigates compliant mechanisms, as well. In Ref. [18], a size optimized periodic vibration isolator was designed with rectangular type compliant inertial amplification mechanisms. In Ref. [19], a two-dimensional periodic vibration isolator was designed with shape optimized compliant inertial amplification mechanisms of rectangular type. In Ref. [26], a size optimized three-dimensional periodic vibration isolator was designed with triangular type compliant inertial amplification mechanisms. In Ref. [27], a periodic vibration isolator was designed with composite triangular type compliant inertial amplification mechanisms. In Ref. [11], a one-dimensional periodic vibration isolator was designed via rectangular type compliant inertial amplification mechanisms with flexure hinge connections. In Ref. [21], a two-dimensional vibration isolator was designed via topologically optimized triangular type compliant inertial amplification mechanisms with flexure hinge connections and instant center of rotation. As seen in the literature review, rectangular or triangular compliant inertial amplification mechanism were studied extensively. However, a simple rhombus type compliant inertial amplification mechanism was not studied yet. To that end, in this article, a simple rhombus type compliant inertial amplification mechanism, which is to be used in the construction of a periodic vibration isolator, is analyzed in detail.

In this study, a parametric study is conducted on various compliant inertial amplification mechanisms. As a result of the parametric study, a mechanism with the highest vibration isolation frequency band width is determined. Then, this selected inertial amplification mechanism is utilized as the unit cell (i.e., the repetitive building block) to construct a periodic vibration isolator, which operates at low frequency region.

2. Model and Methodology

The main objective in this study is to create widest possible vibration isolation frequency band via

inertial amplification method. First, lumped parameter analytical model is discussed to briefly introduce the fundamentals of the method. Then, finite element models are introduced for the parametric studies, in which, three different unit cell configurations are proposed and analyzed. Finally, a periodic medium is created with a selected unit cell mechanism with the widest stop band (i.e., vibration isolation frequency band).

2.1. Analytic model

The lumped parameter inertial amplification mechanism model [7, 8, 18-21] is shown in Figure 1. In this model, k specifies as stiffness, m_a and m are the masses. The connection between m_a and m is rigid. Theta (θ) is the angle between the spring (k) and the rigid connection which combines mass m with mass m_a. The input displacement to the system is y and output displacement is x.

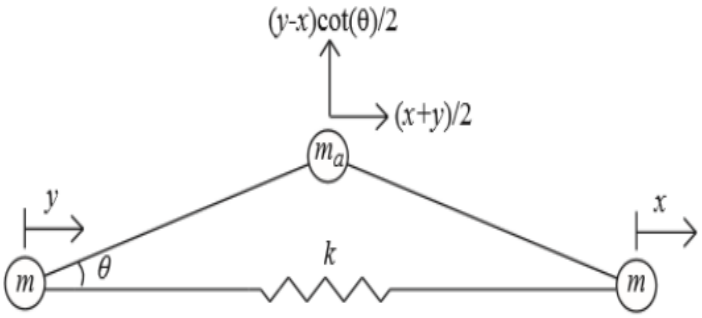

Figure 1. The lumped parameter inertial amplification mechanism model [7, 8, 18-21]

The equation of motion of the inertial amplification mechanism given in Figure 1 is found by the Lagrange method. The Lagrangian expression of the system is equal to the difference of kinetic and potential energies.

The Lagrangian is provided as:

$$L = KE - PE \tag{1}$$

$$\frac{d}{dt}\left(\frac{\partial L}{\partial \dot{x}}\right) - \frac{\partial L}{\partial x} = 0 \tag{2}$$

The kinetic energy of the system is:

$$KE = \frac{m_a}{2}\left(\left(\frac{\dot{x}+\dot{y}}{2}\right)^2 + \left(\frac{\dot{y}-\dot{x}}{2}\,cot\theta\right)^2\right) + \frac{m}{2}\dot{x}^2 + \frac{m}{2}\dot{y}^2 \tag{3}$$

The potential energy of the system is:

$$PE = \frac{1}{2}\,k(x-y)^2 \tag{4}$$

When Equations (3) and (4) are written in their place in Equation (2) and solved, the equation of motion of the system is found as:

$$(m_a(cot^2\theta + 1) + 4m)\ddot{x} + 4kx = m_a(cot^2\theta - 1)\ddot{y} + 4ky \tag{5}$$

In Equation (5), the left side of the differential equation is given with respect to the output x, hence its solution provides the resonance frequency. Similarly, since the right side of the equation is presented with respect to the input y, its solution defines the anti-resonance frequency. As a result, the resonance (ω_1) and the anti-resonance (ω_{z1}) frequencies are as follows:

$$\omega_1 = \sqrt{\frac{k}{m+m_a(cot^2\theta+1)/4}} \tag{6}$$

$$\omega_{z1} = \sqrt{\frac{k}{m_a(cot^2\theta-1)/4}} \tag{7}$$

The beginning of the vibration isolation frequency range of the system is defined as [18, 19]:

$$\omega_s = \sqrt{\frac{2{\omega_1}^2{\omega_{z1}}^2}{{\omega_1}^2+{\omega_{z1}}^2}} \quad (8)$$

As can be seen from Equations (6), (7) and (8), when the angle θ decreases, the vibration isolation starting frequency is reduced, as well. Therefore, low frequency vibration isolation can be achieved.

2.2. Finite element modelling

The compliant inertial amplification mechanism model in this study is shown in Figure 2. The mechanism is formed by using rectangular blocks (enumerated as 1 and 3) and connecting beams (numerated as 2). In other words, the structure is vertically and horizontally symmetric with respect to its (geometric) center. In Figure 2, l and t denote the length and thickness of the corresponding beams of the structure, respectively. The thin beams with length l_2 and thickness t_2 are compliant hinges which provide flexibility and stiffness to the mechanism. Whereas, large blocks of 1 and 3 perform only rigid body motion. Finite element model is created using three dimensional (3D) deformable linear quadrilateral shell elements. ABAQUS software is used for the finite element analysis. Element type selected for the study is S4, which is a fully integrated, general-purpose, finite-membrane-strain shell element. For the compliant inertial amplification mechanism model provided in Figure 2, the total number of finite elements used is 9600. Material type for the finite element model is isotropic.

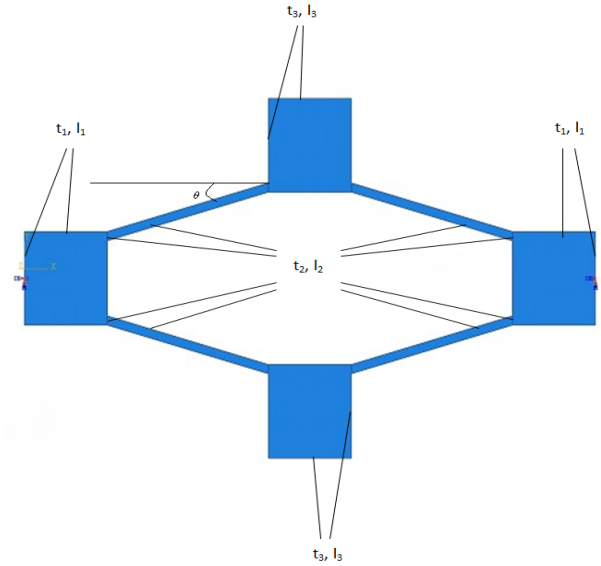

Figure 2. Model of compliant inertial amplification mechanism

2.3. Proposed compliant mechanisms

In this study, various types of compliant inertial amplification mechanisms which have different connection configurations and sizes are analyzed. The aim of the study is to determine how beam sizes and connection configurations affect the vibration isolation frequency range obtained via inertial amplification method. To that end, 2nd beam connection spots are altered and eventually three different compliant mechanism configurations are obtained as presented in Figures 3-5. Parametric studies are conducted on these three mechanisms with different beam sizes (i.e., with different length to thickness ratios for beams) and theta angles (i.e., the acute angle between the horizontal axis and the 2nd beam).

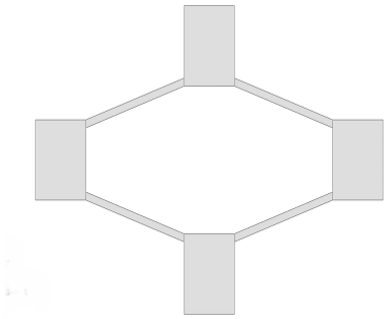

Figure 3. The first compliant mechanism configuration proposed (Mechanism A)

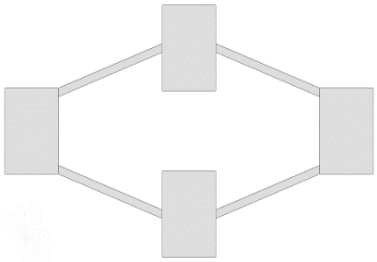

Figure 4. The second compliant mechanism configuration proposed (Mechanism B)

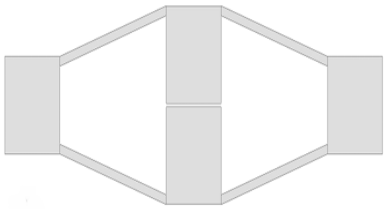

Figure 5. The third compliant mechanism configuration proposed (Mechanism C)

2.4. Parametric studies

The parametric studies are conducted on finite element models of the proposed mechanisms A, B and C which are provided in Figures 3-5. In parametric studies, the effect of alternating beam length to thickness ratios (l/t) and theta angles (θ) on vibration isolation frequency band (band gap) is investigated. In the literature [18-21], it has been shown that the ratio between the second and the first natural frequencies (f_2/f_1) directly demonstrates the band gap width. For this purpose, via modal analysis, natural frequencies of these mechanisms are obtained for various parameters and the ratio of the second natural frequency to the first natural frequency (f_2/f_1) values are tabulated.

First of all, a control structure is determined with parameters given as: $\theta = \pi/12 = 15°$, $l_1 = 5$ m, $t_1 = 5$ m, $l_2 = 10$ m, $t_2 = 0.5$ m, $l_3 = 5$ m, $t_3 = 5$ m.

An isotropic material is considered to be the construction material for the mechanisms. Hence, typical steel material properties are adopted for this purpose. To that end, material property values are selected as follows: modulus of elasticity, $E = 210$ GPa; density, $\rho = 7800$ kg/m^3; Poisson's ratio, $\nu = 0.3$.

The goal in the parametric study is to determine the compliant mechanism structure with the highest f_2/f_1 ratio hence to achieve vibration isolation for maximum frequency band possible.

The variables considered in the parametric study are l_1/t_1, l_2/t_2, l_3/t_3 ratios and θ angle (see Figure 2). After, analyzing f_2/f_1 ratios of the proposed mechanisms (see in Figures 3-5) with various altering parameter values, the mechanisms that have the best f_2/f_1 ratios will be determined for each of the configuration. Ultimately, a last selection will be made among the best of the configurations, to decide the final unit cell mechanism that will be used in the periodic structure.

3. Results and Discussion

3.1. Parametric comparisons of vibration isolation frequency bands

The vibration isolation frequency band characteristics of proposed compliant mechanisms are analyzed and shown in this section. As it is mentioned before in the previous section, control structure parameters are determined and the effect of four variant parameters (θ, l_1/t_1, l_2/t_2 and l_3/t_3) on vibration isolation frequency band width (f_2/f_1) are examined. After examination of trend plots, best parameters for each variant can be determined.

3.1.1. For the first mechanism (Mechanism A)

The first proposed mechanism is shown in Figure 3. To observe vibration isolation frequency band characteristics with altering parameters, trend plots are created (see Figure 6).

In Figure 6 trend plots of the first mechanism (Mechanism A) are presented. It can be seen that when the angle θ increases f_2/f_1 ratio is reduced. Similarly, when l_1/t_1 ratio increases f_2/f_1 ratio decreases. For l_2/t_2, when the ratio increases, f_2/f_1 ratio increases as well. For the last parameter, as l_3/t_3 ratio increases, f_2/f_1 increases as well unless a peak is reached. However, after that critical value, f_2/f_1 is decreased with increasing l_3/t_3 ratio, as opposed to other parameters' trend plots.

3.1.2. For the second mechanism (Mechanism B)

The second proposed mechanism is shown in Figure 4. Besides, corresponding parameter trend plots are on vibration isolation frequency band characteristics of mechanism is given with Figure 7.

For the second mechanism, when θ angle increases f_2/f_1 ratio increases, as well. Different than the first plot, f_2/f_1 ratio decreases when l_1/t_1 ratio increases. In the third trend plot for second mechanism, f_2/f_1 ratio increases when l_2/t_2 ratio increases but the increase on f_2/f_1 ratio decelerating with the l_2/t_2 ratio increase. Same as the first mechanism, f_2/f_1 ratio increases until a critical value for l_3/t_3 ratio is reached and after that it starts to decrease.

3.1.3. For the third mechanism (Mechanism C)

The last proposed mechanism is given by Figure 5. Trend plots of the mechanism is given with the Figure 8.

For the third mechanism, when θ increases f_2/f_1 ratio increase, as well. For l_1/t_1 ratio, trend is different than the first and second mechanisms. Until a certain value of l_1/t_1, f_2/f_1 ratio increase and after that it decreases. When l_2/t_2 ratio increases, f_2/f_1 ratio increases similar to the other mechanisms. For the last trend of third mechanism, f_2/f_1 ratio decrease when l_3/t_3 ratio increase unlike the first two mechanisms.

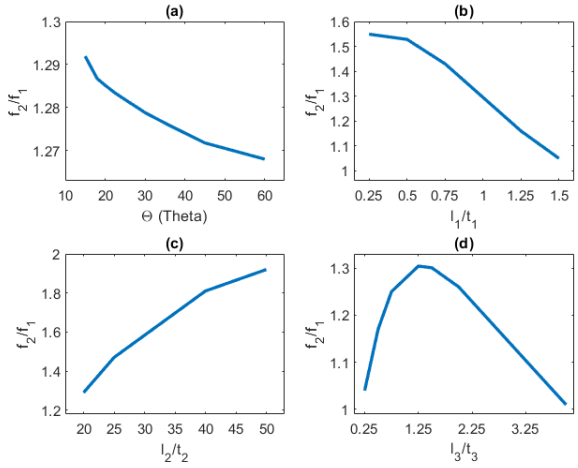

Figure 6. The effect of θ, l_1/t_1, l_2/t_2 and l_3/t_3 parameters on f_2/f_1 ratio for the first mechanism (Mechanism A)

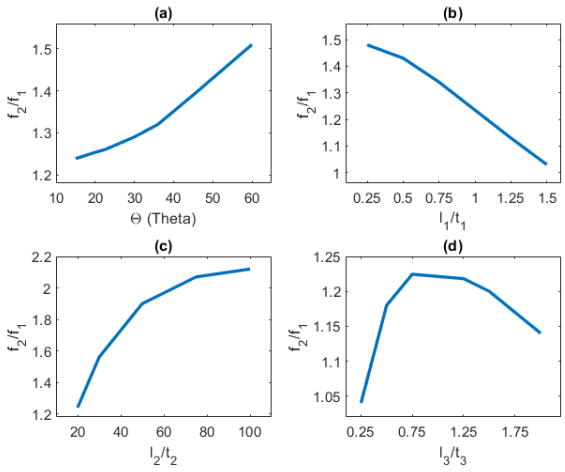

Figure 7. The effect of θ, l_1/t_1, l_2/t_2 and l_3/t_3 parameters on f_2/f_1 ratio for the second mechanism (Mechanism B)

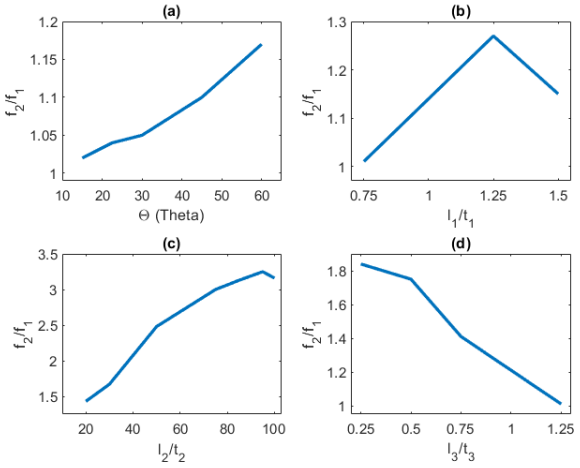

Figure 8. The effect of band gap characteristics theta, l_1/t_1, l_2/t_2 and l_3/t_3 on f_2/f_1 ratio for the third mechanism (Mechanism C)

3.1.4. Discussion on vibration isolation frequency band properties

The results of parametric studies are given with Figures 6, 7 and 8 as trend plots. From here, the best results about vibration isolation frequency band characteristics for all three mechanisms can be found. Moreover, the best vibration isolation frequency band width results (i.e., f_2/f_1 ratios) for each of the proposed configurations (i.e., Mechanism A, B and C) are given with Table 1.

In l_2/t_2 trend plots, it can be seen that f_2/f_1 ratio increases continuously for all mechanism. The reason behind this behavior is when l_2/t_2 ratio increases stiffness of the mechanism decreases hence vibration isolation stop band starting mode (i.e., opening mode (f_1)) is shifted towards lower frequencies. This decrease in stiffness shifts the first mode more than the case observed in the second mode, as a result, f_2/f_1 ratio always increases with increasing l_2/t_2 ratio. However, considering manufacturability of the compliant mechanism beam length to thickness ratio (i.e., l_2/t_2) of mechanisms should be chosen as a realistic value.

In θ trend plots however, one can see a different behavior. For mechanism configuration A (see Figure 6), there is an inverse relationship between θ and f_2/f_1 ratio. Hence the widest possible vibration isolation frequency band is achieved for $\theta = 15°$. It is coherent with the theory, because all of the inertial amplification mass is above the connection line (see Figure 1) and inertial amplification effect is already is at its maximum. On the other hand, for mechanism configurations B and C (see Figures 7 and 8), f_2/f_1 ratio increase with increasing θ. It is due to the fact that, as theory suggests, when inertially amplified mass amount m_a in Figure 1 increases with increasing θ, then inertial amplification effect also increases and vibration isolation frequency band starting frequency f_1 lowers. As a result, f_2/f_1 ratio increases.

The effects of l_1/t_1 and l_3/t_3 ratios on vibration isolation frequency band are similar for Mechanisms A and B as can be seen from Figures 6 and 7. However, the same behavior can not be observed for the Mechanism configuration C. This is an expected result since, Mechanism configuration C's inertial amplification effect is limited. The inertially amplified mass amount has a limit, since, the center of gravity of 3rd block segments almost coincide with the center of gravity of 1st blocks. Hence, Mechanism C's building blocks are almost linear for high l_3/t_3 ratios.

As a summary of the parametric studies, the best values for the parameters θ and l_1/t_1, l_2/t_2, l_3/t_3 ratios are tabulated in Table 1. The candidate unit cell compliant mechanisms for each of the three configurations are determined with respect to Table 1.

Table 1. The best parameter values found, which results with the highest f_2/f_1 ratio, for all of the mechanism configurations

Parameter	Mechanism A	Mechanism B	Mechanism C
Theta (θ)°	15	60	60
l_1/t_1	0.25	0.25	1.25
l_2/t_2	20	20	20
l_3/t_3	1.25	0.75	0.25

The first candidate compliant structure with Mechanism A configuration is shown in Figure 9. Parameters of the mechanism are determined as; $\theta = \pi/12 = 15°$, $l_1 = 1.25$ m, $t_1 = 5$ m, $l_2 = 10$ m, $t_2 = 0.5$ m, $l_3 = 6.25$ m, $t_3 = 5$ m. The first mode of the mechanism (f_1) is at 1.94 Hz and the second mode is (f_2) at 3.54 Hz. According to these modes, f_2/f_1 ratio of candidate mechanism is calculated as 1.83.

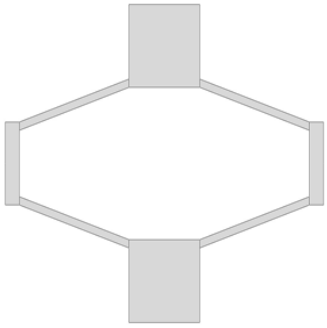

Figure 9. The first candidate mechanism for Mechanism A configuration ($f_2/f_1 = 1.83$)

The second candidate compliant structure with Mechanism B configuration is shown in Figure 10. Parameters of the mechanism are determined as; $\theta = \pi/3 = 60°$, $l_1 = 1.25$ m, $t_1 = 5$ m, $l_2 = 10$ m, $t_2 = 0.5$ m, $l_3 = 3.75$ m, $t_3 = 5$. The first mode of the mechanism (f_1) is at 1.48 Hz, whereas the second mode is (f_2) at 1.58 Hz. With these results, f_2/f_1 ratio of the candidate mechanism calculated as 1.07.

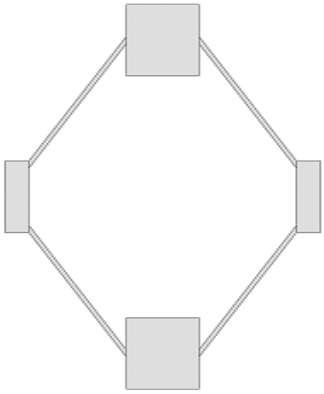

Figure 10. The second candidate mechanism for Mechanism B configuration ($f_2/f_1 = 1.07$)

The third candidate compliant structure with Mechanism C configuration is shown in Figure 11. Parameters of the mechanism are determined as; $\theta = \pi/3 = 60°$, $l_1 = 6.25$ m, $t_1 = 5$ m, $l_2 = 10$ m, $t_2 = 0.5$ m, $l_3 = 1.25$ m, $t_3 = 5$ m. The first mode of the mechanism (f_1) is at 0.97 Hz and the second mode is formed

(f_2) at 1.51 Hz. Calculated f_2/f_1 ratio is equal to 1.55.

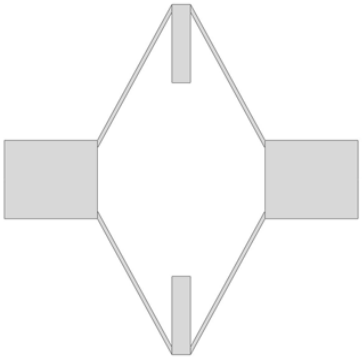

Figure 11. The third candidate mechanism for Mechanism C configuration (f_2/f_1 = 1.55)

After completing modal analysis for candidate configurations, it can be seen that the widest vibration isolation frequency band is achieved via the mechanism provided in Figure 9. Therefore, it is determined as the unit cell for the periodic vibration isolator.

3.2. The unit cell mechanism

The first step of the study was to analyze configurations of all proposed mechanisms and to determine the mechanism, which has the highest f_2/f_1 ratio, as the unit cell of the periodic structure. According to the results, mechanism A configuration was selected as the unit cell. In this step, final dimensions of the unit cell are determined and characteristics of the unit cell mechanism is examined with frequency response function (FRF).

The dimensions of the unit cell given with Figure 12 are determined as: $\theta = \pi/12 = 15°$, l_1 =12.5 mm, t_1 = 50 mm, l_2 = 100 mm, t_2 = 5 mm, l_3 = 62.5 mm, t_3 = 50 mm. The first mode of the unit cell f_1 is seen at 194 Hz and the second mode f_2 is observed at 354.3 Hz. From here, f_2/f_1 ratio is calculated as 1.83.

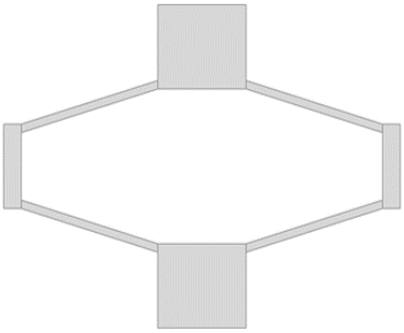

Figure 12. The Unit cell mechanism (f_1 = 194 Hz, f_2 = 354.3 Hz and f_2/f_1 =1.83)

Here, it should be noted that, mode shape frequencies of compliant mechanisms are only a function of l/t ratios and θ values. Therefore, a change on dimensions only causes the mode shape frequencies to shift upwards or downwards provided that the l/t ratios and θ values remain the same [18-21]. As a result, when their ratio stays the same, then f_2/f_1 ratio stays the same, as well (see Figures 9 and 12). Vibration isolation will be achieved between the range of the first two mode frequencies as for the case in the literature [18-21].

In order to characterize the vibration isolation levels of the unit cell mechanism provided in Figure 12, frequency response function (FRF) must be obtained and examined. To that end, a finite element model is created. Roller-roller boundary conditions are applied to the model, which enables the mechanism to move only in the x direction freely at the boundaries. In addition, displacement inputs to the model are provided from the left side in the x direction. As a result, axial displacement inputs are utilized to observe the effect of all modes in the frequency range of interest (0-500 Hz).

The FRF analysis results are presented in Figure 13 as a displacement transmissibility plot. Here, one can see that, the suggested unit cell mechanism in Figure 12 can provide vibration isolation between 194-370 Hz. As can be seen, vibration isolation starting and ending frequencies are closely related with the first and the second mode shape frequencies of the mechanism, which is a result compatible with the literature [18-21]. Within this frequency band (194-370 Hz), at least 25 % vibration isolation can be achieved only by using one mechanism.

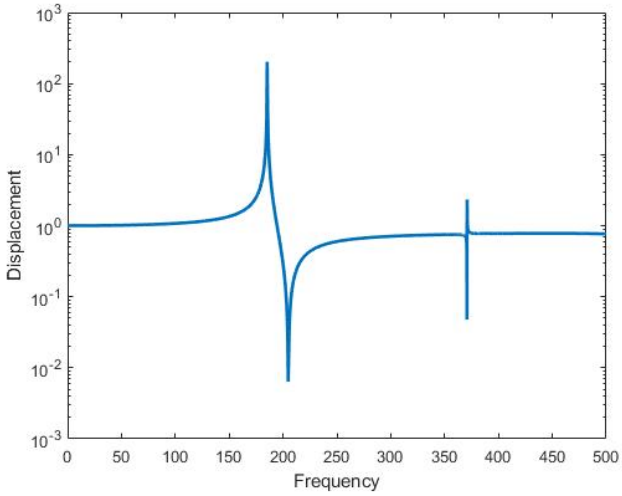

Figure 13. The displacement transmissibility (FRF) of the unit cell mechanism.

3.3. The periodic structure

The goal in this study was to determine a unit cell which provides the highest f_2/f_1 ratio among candidate mechanisms and create a periodic structure with repeated unit cell mechanism. After determination of unit cell mechanism and the geometrical properties for it in the previous section, periodic media can be created and examined properly. As it is previously shown in the literature [18-21], when the number of repeating unit cells in periodic structure is raised then vibration isolation levels achieved via the periodic structure increases, as well. The periodic structure in this study is created with 3 repetition of the unit cell mechanism. Obtained one-dimensional periodic vibration isolator can be seen in Figure 14.

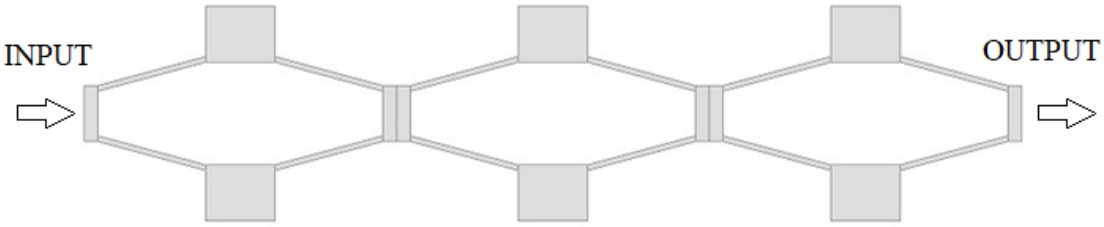

Figure 14. The periodic vibration isolator design.

As indicated in the literature [18-21], it is expected the vibration isolation frequency band starts approximately at 190 Hz, which is the frequency value in the near vicinity of the first mode of the unit cell mechanism, and ends approximately at 360 Hz, which is the frequency value in the near vicinity of the second mode of the unit cell mechanism.

In order to examine the vibration isolation performance of the periodic structure given in Figure 14, the displacement transmissibility (FRF) plot (Figure 15) is calculated with finite element method. Roller-roller boundary conditions are applied as done in the unit cell FRF analysis. Input displacements are provided from one end of the periodic structure and output displacements are taken from the other end (see Figure 14).

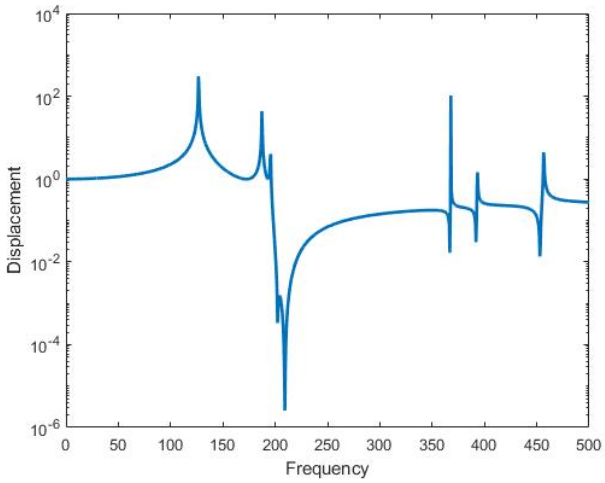

Figure 15. The displacement transmissibility (FRF) of the periodic structure.

It can be seen in Figure 15 that; the periodic structure is performing effective vibration isolation between 190-360 Hz. Despite using only three unit cells in the periodic structure, more than 80 % vibration isolation is achieved throughout the frequency range of interest (i.e., 190-360 Hz). Moreover, if a periodic structure is formed by using more than three unit cell mechanisms, then attained vibration isolation levels will be much higher, as previously shown in the former studies in the literature [18-21]. As a summary, the proposed periodic structure can be utilized as a one-dimensional vibration isolator, in order to mitigate the incoming oscillations from one direction.

4. Conclusion

In this study, a periodic structure, which performs effective vibration isolation at low frequencies, is designed. Firstly, candidate compliant inertial amplification mechanism configurations are proposed and analyzed via parametric studies to determine one of them as the unit cell. Then, a one-dimensional periodic structure is formed by embedding multiple unit cell mechanisms. The periodic structure is analyzed and results obtained from displacement transmissibility (FRF) plots are provided to observe the vibration isolation levels achieved. Considering the results obtained from the study, it is seen that the periodic structure provides effective low frequency vibration isolation for mechanical waves coming from one direction.

However, with this performance, it is also important to consider the manufacturability of these systems. At the present time, modern manufacturing methods such as laser cutting is suitable for producing this kind of monolithic solid mechanism structures, but the production costs will be presumably high. Yet, with developing additive manufacturing methods, it will be possible to produce this kind of periodic vibration isolators with less spending, in the near future.

Acknowledgment

Authors would like to thank Samet Gün for his contribution. Authors would like to give special thanks to Boğaziçi University for providing ABAQUS software usage.

Conflict of Interest Statement

The authors declare that there is no conflict of interest.

References

[1] S. S. Rao, *Mechanical Vibrations*, Upper Saddle River: Prentice Hall, 2011.

[2] S. G. Kelly, *Mechanical Vibrations: Theory and Applications*, Stamford: Cengage Learning, 2012.

[3] D. J. Inman, *Engineering Vibrations*, Upper Saddle River: Pearson Education, 2014.

[4] R. A. Ibrahim, "Recent advances in nonlinear passive vibration isolators," *Journal of Sound and Vibration*, vol. 314, no. 3-5, pp.

371-452, 2008. doi:10.1016/j.jsv.2008.01.014

[5] C. Liu, X. Jing, S. Daley and F. Li, "Recent advances in micro-vibration isolation," *Mechanical Systems and Signal Processing,* vol. 56-57, pp. 55-80, 2015. doi:10.1016/j.ymssp.2014.10.007.

[6] P. S. Balaji and K. K. Selvakumar, "Applications of nonlinearity in passive vibration control: a review," *Journal of Vibration Engineering & Technologies,* vol. 9, pp. 183-213, 2021. doi: 10.1007/s42417-020-00216-3

[7] S. Hao, Z. Wu, F. Li and C. Zhang, "Numerical and experimental investigations on the band-gap characteristics of metamaterial multi-span beams," *Physics Letters A*, vol. 383, no. 36, pp. 126029, 2019. doi:10.1016/j.physleta.2019.126029

[8] L. Zhao, Z. Q. Lu, H. Ding and L. Q. Chen, "Experimental observation of transverse and longitudinal wave propagation in a metamaterial periodically arrayed with nonlinear resonators," *Mechanical Systems and Signal Processing,* vol. 170, pp. 108836, 2022. doi:10.1016/j.ymssp.2022.108836

[9] C. Yilmaz, G. M. Hulbert and N. Kikuchi, "Phononic band gaps induced by inertial amplification in periodic media," *Physical Review B*, vol. 76, no. 5, pp. 054309, 2007. doi: 10.1103/PhysRevB.76.054309

[10] C. Yilmaz and G. M. Hulbert, "Theory of phononic gaps induced by inertial amplification in finite structures," *Physics Letters A*, vol. 374, no. 34, pp. 3576-3584, 2010. doi:10.1016/j.physleta.2010.07.001

[11] S. Taniker and C. Yilmaz, "Generating ultra wide vibration stop bands by a novel inertial amplification mechanism topology with flexure hinges," *International Journal of Solids and Structures,* vol. 106, pp. 129-138, 2017. doi: 10.1016/j.ijsolstr.2016.11.026

[12] A. H. Orta and C. Yilmaz, "Inertial amplification induced phononic band gaps generated by a compliant axial to rotary motion conversion mechanism," *Journal of Sound and Vibration*, vol. 439, pp. 329-343, 2019. doi:10.1016/j.jsv.2018.10.014

[13] C. Xi, L. Dou, Y. Mi and H. Zheng, "Inertial amplification induced band gaps in corrugated-core sandwich panels," *Composite Structures*, vol. 267, pp. 113918, 2021. doi:10.1016/j.compstruct.2021.113918

[14] M. Barys, J. S. Jensen and N. M. M. Frandsen, "Efficient attenuation of beam vibrations by inertial amplification," *European Journal of Mechanics - A/Solids*, vol. 71, pp. 245-257, 2018. doi:10.1016/j.euromechsol.2018.04.001

[15] J. Zhou, L. Dou, K. Wang, D. Xu and H. Ouyang, "A nonlinear resonator with inertial amplification for very low-frequency flexural wave attenuations in beams," *Nonlinear Dynamics,* vol. 96, pp. 647-665, 2019. doi:10.1007/s11071-019-04812-1

[16] S. Chowdhury, A. Banerjee and S. Adhikari, "Enhanced seismic base isolation using inertial amplifiers," *Structures*, vol. 33, pp. 1340-1353, 2021. doi:10.1016/j.istruc.2021.04.089

[17] Y. Zeng, L. Cao, S. Wan, T. Guo, Y. F. Wang, Q. J. Du, B. Assouar and Y. S. Wang, "Seismic metamaterials: generating low-frequency bandgaps induced by inertial amplification," *International Journal of Mechanical Sciences,* vol. 221, pp. 107224, 2022. doi:10.1016/j.ijmecsci.2022.107224

[18] G. Acar and C. Yilmaz, "Experimental and numerical evidence for the existence of wide and deep phononic gaps induced by inertial amplification in two-dimensional solid structures," *Journal of Sound and Vibration*, vol. 332, no. 24, pp. 6389-6404, 2013. doi:10.1016/j.jsv.2013.06.022

[19] O. Yuksel and C. Yilmaz, "Shape optimization of phononic band gap structures incorporating inertial amplification mechanisms," *Journal of Sound and Vibration*, vol. 355, pp. 232–245, 2015. doi:10.1016/j.jsv.2015.06.016.

[20] O. Yuksel and C. Yilmaz, "Size and topology optimization of inertial amplification induced phononic band gap structures," *In Proceedings of the ASME International Mechanical Engineering Congress and Exposition*, 2017, Tampa, Florida, USA, p. V013T01A007. doi:10.1115/IMECE2017-71342

[21] O. Yuksel and C. Yilmaz, "Realization of an ultrawide stop band in a 2-D elastic metamaterial with topologically optimized inertial amplification mechanisms," *International Journal of Solids and Structures*, vol. 203, pp. 138–150, 2020. doi:10.1016/j.ijsolstr.2020.07.018

[22] Z. Cheng, A. Palermo, Z. Shi and A. Marzani, "Enhanced tuned mass damper using an inertial amplification mechanism," *Journal of Sound and Vibration*, vol. 475, pp. 115267, 2020. doi:10.1016/j.jsv.2020.115267

[23] S. Muhammad, S. Wang, F. Li and C. Zhang, "Bandgap enhancement of periodic nonuniform metamaterial beams with inertial amplification mechanisms," *Journal of Vibration and Control*, vol. 26, no. 15-16, pp. 1309-1318, 2020. doi:10.1177/1077546319895630

[24] J. Li, P. Yang and S. Li, "Phononic band gaps by inertial amplification mechanisms in periodic composite sandwich beam with lattice truss cores," *Composite Structures,* vol. 231, pp. 111458, 2020. doi:10.1016/j.compstruct.2019.111458

[25] N. M. M. Frandsen, O. R. Bilal, J. S. Jensen and M. I. Hussein, "Inertial amplification of continuous structures: Large band gaps from small masses", Journal of Applied Physics, vol. 119, pp. 124902, 2016. doi: 10.1063/1.4944429

[26] S. Taniker and C. Yilmaz, "Design, analysis and experimental investigation of three-dimensional structures with inertial amplification induced vibration stop bands," *International Journal of Solids and Structures*, vol. 72, pp. 88-97, 2015.

doi:10.1016/j.ijsolstr.2015.07.013

[27] K. Mizukami, K. Funaba and K. Ogi, "Design and three-dimensional printing of carbon-fiber-composite elastic metamaterials with inertial amplification mechanisms," *Journal of Sound and Vibration,* vol. 513, pp. 116412, 2021. doi:10.1016/j.jsv.2021.116412

This is an open access article under the CC-BY license